Ribosome hijacking: a role for small protein B during trans-translation

Sylvie Nonin-Lecomte, Noëlla Germain-Amiot, Reynald Gillet, Marc Hallier, Luc Ponchon, Frédéric Dardel, Brice Felden

Ribosome hijacking: A role for small protein B during *trans*-translation

Sylvie Nonin-Lecomte[*†‡], Noella Germain-Amiot[‡§], Reynald Gillet[§], Marc Hallier[§], Luc Ponchon*, Frédéric Dardel* & Brice Felden [†§]*

[*]Université Paris Descartes, Laboratoire de Cristallographie et RMN Biologiques, CNRS UMR 8015, 4, av. de l'Observatoire 75006 Paris and [§]Université de Rennes I, UPRES JE2311, Inserm U835, Biochimie Pharmaceutique, 2 av. du Prof. L. Bernard 35043 Rennes, France. [‡]The authors contributed equally to the work. [†]joint correspondence: sylvie.nonin@univ-paris5.fr; bFelden@univ-rennes1.fr

Tight recognition of codon-anticodon pairings by the ribosome ensures accuracy and fidelity of protein synthesis. In eubacteria, translational surveillance and ribosome rescue is performed by the "tmRNA-SmpB" system (transfer messenger RNA-Small protein B). Remarkably, entry and accommodation of aminoacylated-tmRNA into stalled ribosomes occur without a codon-anticodon interaction but in the presence of SmpB. We show that within a stalled ribosome, SmpB interacts with the three universally conserved bases G530, A1492 and A1493 that form the 30S subunit decoding centre, in which canonical codon-anticodon pairing occurs. The footprints at positions A1492 and A1493 of a small DC, and on a set of conserved SmpB amino acids, were identified by NMR. Mutants at these residues present same growth defects as for *ΔsmpB* strains. The SmpB protein has functional and structural similarities with initiation factor 1. SmpB is proposed to be a functional mimic of the pairing between a codon and an anticodon.

Characters: 27058

Keywords: Ribosome | decoding | trans-translation | tmRNA | SmpB

Abbreviations: BR: binding region; c.o.: cut-off; CSP: chemical shift perturbation; DC: decoding centre; DMS, dimethylsulfate; eq.: equivalent; HSQC: heteronuclear single quantum coherence spectroscopy; NMR: nuclear magnetic resonance; NOESY: nuclear Overhauser effect spectroscopy; ppm: parts per million; su: subunit; TLD: tRNA-like domain; TOCSY: total correlation spectroscopy; WACS: weighted-average chemical shifts; wt: wild type.

INTRODUCTION

Protein synthesis occurs within the ribosome according to the rules of the genetic code (Fig. S1a). The 30S subunit ensures the selection of the correct aminoacylated-transfer RNAs (aa-tRNAs). The 50S su catalyzes the formation of the peptide bond. The decoding center (DC) of the genetic information is within the 30S su. Translational accuracy and fidelity are ensured by key conserved nucleotides (Noller, 2006; A1492, A1493 of helix h44 and G530 of helix h18 of the 16S rRNA), which recognize the minihelix formed by the pairing of the cognate tRNA anticodon and the mRNA (Ogle & Ramakrishnan, 2005). This induces a domain closure of the 30S for cognate tRNA and leads to GTP hydrolysis by elongation factor Tu (EF-Tu) ~75Å away, allowing the acceptor branch of the tRNA to be accommodated into the acceptor A-site of the 50S su and the chemistry of peptidyl transfer to proceed.

In eubacteria and some organelles, these universal rules are temporarily broken during *trans*-translation, a translational surveillance mechanism, when the tmRNA-SmpB system (**t**ransfer **m**essenger **RNA**-**Sm**all **p**rotein **B**) performs the rescue of ribosomes stalled on defective mRNAs. The Ala-tmRNA functions as both a tRNA and an

mRNA. With the help of SmpB and EF-Tu, it binds to the stalled ribosomes. Translation switches from mRNA to a short tmRNA internal open reading frame that encodes a degradation tag, leading successively to a normal termination, the release of the tagged polypeptide and the disassembly and recycling of ribosomal subunits (Moore & Sauer, 2007). SmpB is an OB-fold protein. Its C-terminal tail is essential for function (Jacob *et al,* 2005), but its structure is disordered outside the ribosome. Phylogenetically conserved residues define two surface patches on opposite sides of SmpB (Dong *et al,* 2002). One coincides with the surface that binds to the elbow region of the TLD (Gutmann *et al,* 2003), and the other most likely contacts the ribosome.

Strikingly, the entry and accommodation of Ala-tmRNA into the A-site of a stalled ribosome occur in the absence of any codon-anticodon interaction. Indeed, tmRNA lacks an anticodon loop and it can only enter the ribosome when the A-site is vacant. How can it bypass the decoding process and be accommodated for transpeptidation is unknown. Solution probing (Kurita *et al,* 2007), cryo-EM, (Gillet *et al,* 2007) and X-ray structures (Gutmann *et al,* 2003; Bessho *et al,* 2007) suggest that when *trans*-translation initiates, one SmpB substitutes for a tRNA anticodon stem-loop within the A-site (Fig. S1b). *In vivo*, SmpB is associated with the stalled ribosomes independently of the presence of tmRNA and pre-binding of SmpB to stalled ribosomes triggers *trans*-translation (Hallier *et al,* 2006).

In this report, we show by chemical probing that the protein modifies the conformation of the universally conserved nucleotides A1492, A1493 and G530 of a stalled ribosome, and that the essential C-ter tail of the protein interacts with G530 but is dispensable for the recruitment of tmRNA. We show that 30S mutants at these individual positions still bind SmpB, indicating that the molecular recognition of the protein involves additional residues from the ribosome. By NMR, within a ternary [TLD/SmpB/DC] complex, we identify interacting DC nucleotides and SmpB residues. We show that strains expressing mutant SmpBs modified at the interacting positions present the same growth defects as those inactivated in *trans*-translation. Based on these data, a model of the interaction between the SmpB-TLD complex and the ribosomal A-site of the 30S subunit is inferred.

RESULTS

SmpB induces reactivity changes of nucleotides forming the decoding site. We focused on the 16S rRNA loop 530 (h18) and on the top of h44 within stalled ribosomes, where SmpB roughly fits into the cryo-EM maps (Gillet et al, 2007). In the absence of SmpB, G530 N1 and N2 are accessible to methylation by kethoxal. In the presence of wtSmpB, the reactivity decreases by ~80% (Fig. 1a). The binding of a mutant deleted from the last 16 aminoacids (Δ-Cter ecSmpB) leaves G530 accessible to modifications, showing that the C-ter tail of SmpB either protects G530 or induces conformational changes at this position (not shown). Similarly, A1492 N1 and A1493 N1within the stalled ribosome are accessible to DMS modifications (Fig. 1b), and their accessibility is reduced by ~80% upon binding of wt ecSmpB. We conclude that SmpB reacts as a tRNA anticodon mimic during decoding by inducing reactivity changes at positions A1492, A1493 and G530..

Binding of SmpB to *E. coli* small subunits containing point mutations in the 16S rRNA. Reactivity changes at G530, A1492 and A1493 upon SmpB binding to a stalled ribosome led us to test SmpB binding to 30S su carrying single point mutations at each of these bases. The A1492G, A1493G and G530A mutations all result in dominant lethality and general translation defects in *E. coli*. Each 30S mutant binds to SmpB similarly as the wt 30S (Fig. 1c),

suggesting that the individual contributions of the three nucleotides to the molecular recognition of the 30S su by SmpB are negligible. Filter binding assays with labelled tmRNA, in complex with a stalled ribosomal complex preloaded with either wt or Δ–Cter ecSmpB, were performed to check whether the C-terminus of SmpB influences tmRNA recruitment. The efficiency of both proteins is comparable (Fig. 1d), showing that the 16 C-terminal residues are dispensable during this early step, but seem required for pseudo-decoding (Fig. 1a).

SmpB interacts simultaneously with tmRNA TLD and the DC. Ala-tmRNA accommodation proceeds in the absence of specific recognition by a complementary anticodon. Based on structural data, the RNA binding site of the protein for the ribosomal DC is predicted to be different from that of the TLD. We used the (1:1) [Δ–Cter SmpB/TLD60] complex to probe the SmpB/DC interaction, focusing on a minimal decoding site encompassing A1492 and A1493 but excluding G530. The choices of the RNA sequences (DC27 and DC33, Fig. 3) and of the protein (the *A. aeolicus* Δ–Cter SmpB) are explained in Supplementaries. Changes in the structure or dynamics of Δ–Cter SmpB and of DC33 upon complex formation were probed using NMR under stringent ionic conditions (450mM NaCl). The association of ^{15}N-labeled SmpB with TLD60 was monitored in a ^{1}H-^{15}N HSQC spectrum (Fig S2a). The NMR data are consistent with previous studies on the [SmpB/TLD] complex (Nameki et al, 2005; Bessho et al, 2007). Interacting residues are conserved among bacteria and are clustered on the "top face" of the protein (Fig. S3) within a region we called « Binding Region 1 » (BR1, supplementary text).

We monitored the changes in the ^{15}N-^{1}H HSQC spectrum of SmpB upon addition of up to 8 eq. of unlabeled DC27 RNA, using the (1:1) [Δ–Cter SmpB/TLD60] complex as reference (Figs. 2a and S4a). The induced CSP (Fig. 2b) show a second binding region (BR2) within the "bottom face" of the protein, opposite to BR1, clustering along a stretch extending from L110 to K129, including residues Y20, L110, L112, K127 and K129 which are evolutionary conserved.

The CSP in BR2 (Fig S4a) originate from direct and indirect effects. Most residues of helix α1 (E15, A16, K19 and Y20) are strongly affected.. Additional CSP are located on beta sheets 6 (L110 and L112) and 7 (K118 and A124), both surrounding helix α1. In the free protein, the side chains of L110 and A124 point towards A16, forming hydrophobic interactions that could sense conformational changes in helix α1 upon binding of the DC. E102 from helix α3 is ~17Å away from K19, compatible with the distance spacing A1492 and C1402 phosphorus atoms. K127, K129 and R134 are located in the flexible C-terminal part of the protein protruding from beta sheet 7, next to helix α1. Any conformational change within beta sheet 7 is expected to affect the conformation of the C-ter tail of SmpB. Also, these three basic residues could interact with the DC.

The [SmpB-TLD] complex induces a conformational change of the decoding site RNA. Up to 8 eq. of the (1:1) [Δ–Cter SmpB/TLD60] complex were added to ^{13}C,^{15}N-DC33 RNA in D_2O buffer. The corresponding ^{13}C-^{1}H HSQC spectra were compared to that of the free DC33 (Fig. 3). The conformational changes induced by the protein extend to G1494 with its H8 resonance undergoing the largest CSP (Fig. 3b). The aromatic resonances of neighboring G1491 and of A1408, which are part of the DC, also shift to a lesser extent. The insignificant CSP observed for G1405 H8, G1497 H8, A1410 H8/H2, G1489 H8, G1488 H8 and g15 (not shown) demonstrate the preferential binding of SmpB to the decoding site and not to the abutting stems. A1493 H8 CSP are larger than that of A1492 H8 (Fig. 3c), in agreement with the probing data collected on a 70S ribosome (this work).

Mutations of residues in the BR2 lead to *trans*-translation deficient phenotypes *in vivo*. It is inferred from the NMR data that E15, K19, Y20, K127 and K129 of the *A. aeolicus* SmpB play a role in the interaction with the DC.

The biological relevance was assessed *in vivo* using *E. coli* Δ*smpB* strains complemented with ecSmpB mutants. Residues R19, E23, Y24, K131 and K133 are the homologues of the *A. aeolicus* E15, K19, Y20, K127 and K129, respectively. We constructed R19A/E23A/Y24A (ecSmpB-REY) and K131A/K133A (ecSmpB-KK) mutants. Complementation of a Δ*smpB* strain with either *wt ecsmpB*, *ecsmpB-REY* or *ecsmpB-KK* genes yields similar levels of protein expression (not shown). As for wt ecSmpB, the two ecSmpB variants associate to the 70S (the P100 fraction) and to tmRNA *in vivo* (Fig. S5a). They however fail to complement the growth defect of the Δ*smpB* strain at 45°C (Fig. S5b) . The ecSmpB protein mutated at five residues from BR2, predicted from our NMR data to interact with the DC, bind the 70S and tmRNA but present a *trans*-translation deficient phenotype *in vivo*.

Model of the 'SmpB-TLD-70S ribosome' complex. We combined the published crystallographic data with our work to propose a model of the 'SmpB-TLD' complex into a 70S ribosome, consistent with the one reported by Bessho et al. (2007) and with the cryo-EM data (Kaur et al, 2006), and with all our NMR and probing results. The docking procedure is described in the Supplementaries. In the resulting model (Fig. 4) SmpB fills the space normally occupied by the anticodon stem-loop of the A-site tRNA. The localisation of helix alpha 1 and of some conserved residues at the end of beta sheet 7 suggest that these parts of SmpB can contact A1492, A1493 and G530.

DISCUSSION

SmpB mimics a codon-anticodon pairing in *trans*-translation. Recent cryo-EM reconstructions (Gillet *et al,* 2007) and hydroxyl radical probing of the interaction between SmpB and ribosomes (Kurita *et al,* 2007) suggest that SmpB binds the 30S near the DC (Fig. S1). Our structural and biochemical data suggest that the tmRNA-SmpB complex acts as a 'codon-anticodon' mimic during transpeptidation of the stalled polypeptide to the tmRNA alanine. Conserved G530, A1492 and A1493 contact a cognate 'codon–anticodon' pair by induced fit during decoding. We show here that SmpB protects the WC positions of these three bases within a stalled ribosomal complex, as does a tRNA anticodon stem-loop. Each of these bases can be mutated without impairing the binding of SmpB to the ribosome, implying that their contributions to binding are limited. Although having no contributions to tmRNA recruitment to the ribosome, the C-terminus of SmpB is essential for *trans*-peptidation (Hallier *et al,* 2006). The absence of *trans*-translation when the SmpB C-tail is lacking is due to defects occurring after tmRNA recruitment but before or during *trans*-peptidation. The NMR data using a ΔC-ter SmpB supports a suggested orientation of the protein in which its globular body interacts with the top of h44 containing A1493, while its C-tail points towards h18, along with the mRNA path (Kurita *et al,* 2007). Our data suggest that the C-tail of SmpB has important contribution during pseudo-decoding, thanks to interactions with G530. Close interactions of the C-terminal extension in the vicinity of G530 may help triggering pseudo-decoding.

Similarities between SmpB and IF1. Our data are consistent with functional conformational changes of the three conserved bases from the DC upon SmpB binding to the stalling complex. Remarkably, our NMR and probing data show that the conformation of A1492 and A1493 is modified in the presence of a 'TLD-SmpB' complex. Until now, these changes were detected upon pairing of an mRNA codon to a tRNA anticodon (Ogle *et al,* 2001), upon binding of IF1 (Carter *et al,* 2001) or of aminoglycosides (Fourmy *et al,* 1998; Ogle *et al,* 2001). Both SmpB and IF1 are members of the S1 family of OB fold proteins (Dong *et al,* 2002). IF1 interacts with the 30S, especially within the DC, *via* a loop inserting into the h44 minor groove and flipping out bases A1492 and A1493, and tight interactions with the phosphate backbone of the h18 G530 loop. A1492G and A1493G ribosomal mutations disrupt IF1 binding to the 30S, while G530A allows it. Conversely and as shown here, the SmpB binding is retained, suggesting that the protein has additional anchor points including its C-terminal domain. The IF1 structure in complex with the DC

(PDB 1HRO) was docked into our stalling model by superimposing the DC internal loops from the 16S rRNA (Fig. 4, inset). Strinkingly, an alpha helix rich in basic residues is found in the vicinity of both IF1 and SmpB interacting domains with the DC, even though the orientations of the two helices are different. Moreover, the positioning of R41 and R46 in IF1 and the distance in beetween them are consistent with the identified residues of BR2. Our model suggests that residues E15, K19 and Y20 induce/stabilize A1492 and A1493 conformational changes, as for IF1 R41 and R46. The functional relevance of our structural results was supported by an *E. coli* strain expressing the A19-A23-Y24 triple ecSmpB mutant that has a growth defect similar to that of a ΔSmpB strain (Fig. S5b), supporting the essential role of some (or all) of these residues for the function of SmpB. In the ternary complex, significant CSP were also observed for K127, K129 and R134 (Fig. 3), expected to interact with the DC (Fig. 4). Our model orientates K127 and K129 towards G530 and towards the mRNA path (Fig. 4), suggesting they might guide for the correct positioning of SmpB within an empty A-site.

It is likely that SmpB reorientates slightly during accommodation. We hypothesize that this would drive conformational changes within the TLD that could be the trigger for GTP hydrolysis and subsequent peptidyl transfer. The fate of SmpB after translocation of tmRNA to the P-site is of a particular interest. A second binding site for SmpB is present within the 30S P site (Ivanova *et al,* 2005; Kurita *et al,* 2007). After peptidyl-transfer, the translocation of tmRNA to the P-site may occur in complex with SmpB, still mimicking a 'codon-anticodon' interaction. Such a model would allow the exit of the protein from the ribosome by the E-site, after an additional round of translation.

METHODS

Preparation and Purification of the complexes. Complexes of *E. coli* ribosomes with P-site tRNA stalled on the rGGCAAGGAGGUAAAAAUG mRNA sequence and mutant 30S subunits were prepared as described (Valle *et al,* 2003; Hallier *et al,* 2006), respectively using a 4-fold or a 2-fold excess of either wt or Δ–Cter (Hallier *et al,* 2006) SmpBs. The protein was incubated for 15min at 37°C and purified on a Superdex 200 HR 10/30 column (GE Healthcare). Anti-SmpB western blots were performed as in Hallier *et al,* (2006).

Chemical modifications. DMS and kethoxal methylations were achieved as in Stern *et al,* (1988). Primer extensions were performed using 5'-ACGGTTACCTTGTTA-3' and 5'-CGTGCGCTTTACGCCCA-3', complementary to nts 1512-1498 and 565-581 of 16S rRNA respectively. Annealing to the purified rRNA was in Tris-HCl 50mM pH8.3, NaCl 60mM, DTT 10mM by heating at 96°C for 40s followed by ice freezing for 1min. Extension was performed by adding 0.5U of the AMV RT in Tris-HCl 50mM pH8.3, NaCl 60mM, 6mM MgCl2, DTT 10mM. After 30 min at 45°C, samples were analyzed by PAGE together with the sequencing of the *E. coli* 16S rRNA.

Equilibrium dissociation experiments. After folding, 2 µl [γ^{32}P]tmRNA were added to the ribosomal complexes and let 5 min at 20 °C, in 15µl of 5mM Hepes-KOH, pH 7.5, 50mM KCl, 10mM NH4Cl, 10mM MgOAc and 6mM β-mercaptoethanol. The samples were diluted with 500µl of ice cooled buffer and filtered over nitrocellulose filters and washed with 3x1 ml of the same buffer. Membranes were dried and radioactivity was measured (Wallac 1409).

NMR. DC27 RNA was purchased from Perbio Inc. ^{13}C-^{15}N DC33, TLD60 and the *A. aeolicus* Δ–Cter SmpB were overproduced and purified as in Gutmann *et al,* (2003); Gaudin *et al,* (2003); Ponchon & Dardel (2007). The NMR buffer for the pure RNA and protein samples is 95%H_2O-5% H_2O, 450mM NaCl, 0.1mM EDTA, pH 6.5. When necessary, H_2O was exchanged to D_2O. The concentration of the reference molecule was set to 0.2 mM. All RNA sample tubes were heated and snap-cooled before NMR experiments. Spectra were recorded on a 600MHz Bruker advance spectrometer equipped with a TXI probe, using 5mm Shigemi NMR tubes, processed with NMRPipe

(Delaglio *et al,* 1995) and analyzed with Sparky. Specific amide NH assignments were checked and reassigned based on the assignments at lower salt concentration and standard ^{1}H-^{15}N HSQC, ^{15}N NOESY-HSQC and ^{15}N TOCSY-HSQC experiments. The NMR titration protocol is provided as supporting information. The changes in the chemical shifts of the amide ^{1}H and ^{15}N were averaged by using the formula: $wacs = \{[1/2[(\Delta H)^2 + (0.2\Delta N)^2]]\}^{1/2}$ (Foster *et al,* 1998) and plotted versus the residue number. The cutoff value (c.o.) of $\square+\sigma$ was computed. All residues undergoing wacs > c.o. were mapped in red on the structure, and those with wacs in the ranges [c.o. - 90% c.o] and [90% c.o. - 80% c.o.] respectively in orange and yellow. Amino acids with NH cross-peak broadened to baseline were mapped in magenta. The structures of the ribosome, of SmpB and of IF1 proteins were displayed using PYMOL (Delano, 2002) and subjected to manual docking as explained in the supplementaries.

ACKNOWLEDGMENTS

We are grateful to Dr A. Méreau (UMR6061, Rennes) for help on the probing experiments, and Bili Seijo (UMR8015) for help on samples preparation. The 30S mutants were provided by Dr R. Green (Johns Hopkins University, USA). This work was supported by grants from Région Bretagne (PRIR Grant n°691 and CRB 2004-1483), ACI BCMS 136 and ANR programme MIME 2006 to BF.

FIGURE LEGENDS

Fig. 1: (a, b) Mapping of accessible Gs and As of *E. coli* 16S rRNA within a stalled ribosome respectively by Kethoxal (A) and DMS (B). *Top*: Autoradiograms of 12% polyacrylamide gels of the cleavage products of extended cDNAs. Lanes U, G, C, and A: sequencing ladders. *Bottom:* Quantization of the protections. **(c)** Imunoblotting of *stalling* "truncated mRNA-tRNA^{fMet}-30S-SmpB" complexes from wt 30S or mutants at positions 530, 1492 and 1493. **(d)** Equilibrium dissociation experiments of tmRNA on stalled ribosomes from filter-binding assays, with maximum binding set to 1, and the other values expressed as the bound fraction: stalled 70S pre-loaded with wt SmpB (diamonds) or with Δ-Cter SmpB (squares).

Fig. 2: DC27 binds to Δ–Cter SmpB region BR2. (**a**) Overlay of the ^{1}H-^{15}N HSQC spectra of Δ-Cter SmpB in the (1:1) [TLD60/Δ–Cter SmpB] complex (blue) and in the (1:1:8) [TLD60/Δ–Cter SmpB/DC27] complex (red). (**c**) Mapping of the perturbations onto the structure of SmpB (PDB 1K8H1) using the color code described in the methods. BR2 is circled in grey.

Fig. 3: Titration of ^{13}C, ^{15}N-DC33 with (1:1) [TLD60/Δ–Cter SmpB]. (**a**) 2D structures of DC27 (boxed) and DC33. The three (DC27) or six (DC33) upper G-C base-pairs as well as nucleotides 'uucg' from the apical loop increase the stability of the RNA stem-loop and are not present in the natural sequences. (**b, c, d**) Overlays of selected regions of the ^{13}C-^{1}H HSQC spectra of the free RNA (black) and of ^{13}C, ^{15}N-DC33 in the presence of 8 eq. of the (1:1) [TLD60/Δ–Cter SmpB] complex (red): GH8 and AH8 regions (panels b and c); AH2 region (panel d).

Fig. 4: Model of the DC-SmpB interaction within the ribosome: 50S and 30S subunits surfaces from a *Thermus thermophilus* ribosome are coloured respectively in cyan and pale green, E-site and P-site tRNAs in red and orange, mRNA in blue, the TLD in grey and SmpB in blue. The parts of h44 and h18 involved in the decoding are shown in ribbon mode (pink and yellow). Adenines 1408, 1492, 1493 from h44 and G530 from h18 are in red. BR2 SmpB amino acids are colored as in Fig. 3. ***Inset:*** Comparison with the IF1 structure (purple) with the decoding site (pink, PDB 1HR0). Red: DC A1408, A1492 and A1493. Cyan: R41 and R46 stack respectively against the A1492 and A1493.

REFERENCES

Bessho Y, Shibata R, Sekine S, Muruyama K, Higashijima K, Hori-takemoto C, Shirouzu M, Kuramitsu S, Yokoyama S (2007) Structural basis for functional mimicry of long-variable-arm tRNA by transfer-messenger RNA. *Proc Natl Acad Sci USA* **104:** 8293-8298

Carter A., Clemons Jr WM, Brodersen DE, Morgan-Warren RJ, Hartsch T, Wimberly BT, Ramakrishnan V (2001) Crystal structure of an initiation factor bound to the 30S ribosomal subunit. *Science* **291:** 498-501

Delaglio F, Grzesiek S, Vuister GW, Zhu G, Pfeifer J, Bax A (1995) NMRPipe: a multidimensional spectral processing system based on UNIX pipes. *J Biomol NMR* **6:** 277–293

DeLano WL (2002) The PyMOL Molecular Graphics System. San Carlos, CA: DeLano Scientific LLC. http://www.pymol.org

Dong G, Nowakowski J, Hoffman DW (2002) Structure of small protein B: the protein component of the tmRNA-SmpB system for ribosome rescue. *EMBO J.* **21:**1845-1854

Foster MP, Wuttke DS, Clemens KR, Jahnke W, Radhakrishnan I, Tennant L, Reymond M, Chung J, Wright, PE (1998) Chemical shift as a probe of molecular interfaces: NMR studies of DNA binding by the three amino-terminal zinc finger domains from transcription factor IIIA. *J Biomol NMR* **12:** 51–71

Fourmy D, Recht MI, Puglisi JD (1998) Binding of neomycin-class aminoglycoside antibiotics to the A-site of 16 S rRNA. *J Mol Biol* **277:** 347-362

Gaudin C, Nonin-Lecomte S, Tisné C, Corvaisier S, Bordeau V, Dardel F, Felden, B (2003) The tRNA-like domains of *E coli* and *A. aeolicus* transfer-messenger RNA: structural and functional studies. *J Mol Biol* **331:** 457-471

Gillet R, Kaur S, Li W, Hallier M, Felden B, Frank J (2007) Scaffolding as an organizing principle in trans-translation. *J Biol Chem* **282:** 6356-6363

Gutmann S., Haebel PW, Metzinger L, Sutter M, Felden B, Ban N (2003) Crystal structure of the transfer-RNA domain of transfer-messenger RNA in complex with SmpB. *Nature* **424:** 699-703

Hallier M, Desreac J, Felden B (2006) Small protein B interacts with the large and the small subunits of a stalled ribosome during trans-translation. *Nucleic Acids Res* **34:** 1935-43

Ivanova N, Pavlov MY, Bouakaz E, Ehrenberg M, Schiavone LH (2005) Mapping the interaction of SmpB with ribosomes by footprinting of ribosomal RNA. *Nucleic Acids Res* **33:** 3529-3539

Jacob Y, Sharkady SM, Bhardwaj K, Sanda A, Williams KP (2005) Function of the SmpB tail in transfer-messenger RNA translation revealed by a nucleus-encoded form. *J Biol Chem* **280**: 5503-5509

Kaur S, Gillet R, Li W, Gursky R, Frank J (2006) Cryo-EM visualization of transfer messenger RNA with two SmpBs in a stalled ribosome. *Proc Natl Acad Sci USA* **103:**16484-16489

Kurita D, Sasaki R, Muto A, Himeno H (2007) Interaction of SmpB with ribosome from directed hydroxyl radical probing. *Nucleic Acids Res* **35:**7248-7255

Moore SD, Sauer RT (2007) The tmRNA system for translational surveillance and ribosome rescue. *Annu Rev Biochem* **76:** 101-124

Nameki N, Someya T, Okano S, Suemasa R, Kimoto M *et al.* (2005) Interaction analysis between tmRNA and SmpB from *Thermus thermophilus*. *J Biochem* **138:** 729-739

Noller HF (2006), *in The RNA world (3rd edn),* eds Gesteland RF, Cech TR, Atkins JF (Cold Spring Harbor Laboratory Press, Cold Spring Harbor, New York), Chap. 10, 287-307.

Ogle JM, Brodersen DE, Clemons WM Jr, Tarry MJ, Carter AP, Ramakrishnan V (2001) Recognition of cognate transfer RNA by the 30S ribosomal subunit. *Science* **292:** 897-902

Ogle JM, Ramakrishnan V (2005) Structural insights into translational fidelity. *Annu. Rev. Biochem* **74:** 129-177

Ponchon L, Dardel F (2007) Recombinant RNA technology: the tRNA scaffold. *Nat Methods* **4:** 571-576

Someya T, Nameki N, Hosoi H, Suzuki S, Hatanaka H, Fujii M, Terada T, Shirouzu M, Inoue Y, Shibata T, Kuramitsu S, Yokoyama S, Kawai G (2003) Solution structure of a tmRNA-binding protein, SmpB, from *Thermus thermophilus*. *FEBS Lett* **535:** 94-100

Stern S, Moazed D, Noller HF. (1988) Structural analysis of RNA using chemical and enzymatic probing monitored by primer extension. *Methods Enzymol* **164:** 481-489

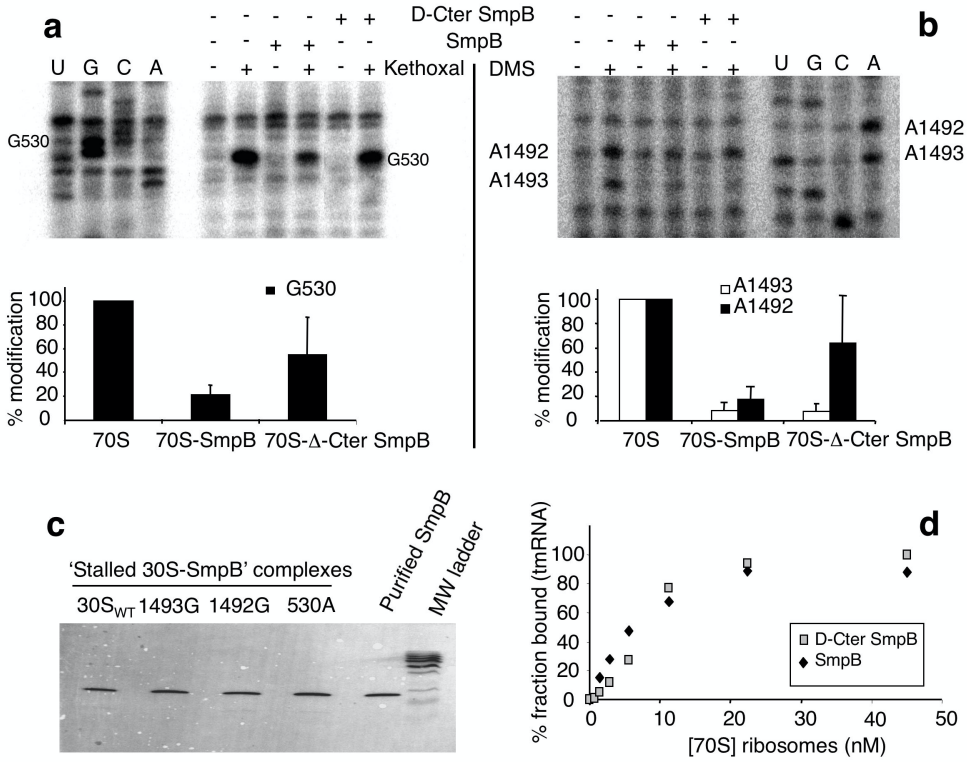

Fig. 1

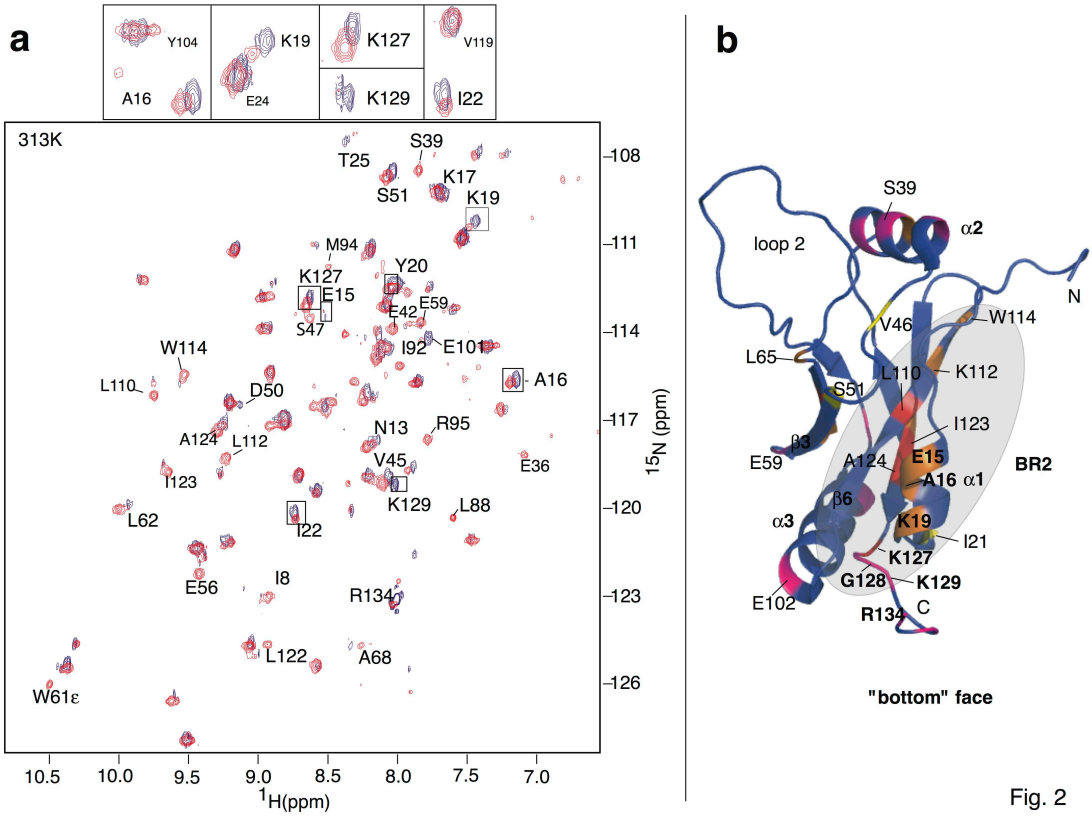
a
Y104
A16
K19
E24
K127
K129
V119
I22
313K
T25
S39
K17
S51
K19
M94
Y20
K127
E15
E42
E59
S47
I92
E101
W114
L110
D50
A16
N13
R95
A124
L112
V45
E36
I123
K129
L88
L62
I22
E56
I8
R134
L122
A68
W61ε
108
111
114
117
120
123
126
15N (ppm)
10.5
10.0
9.5
9.0
8.5
8.0
7.5
7.0
1H(ppm)
b
S39
α2
loop 2
N
V46
W114
L65
L110
K112
S51
I123
β3
E59
A124
E15
BR2
A16 α1
β6
α3
K19
I21
K127
G128
K129
E102
R134
C
"bottom" face

Fig. 2

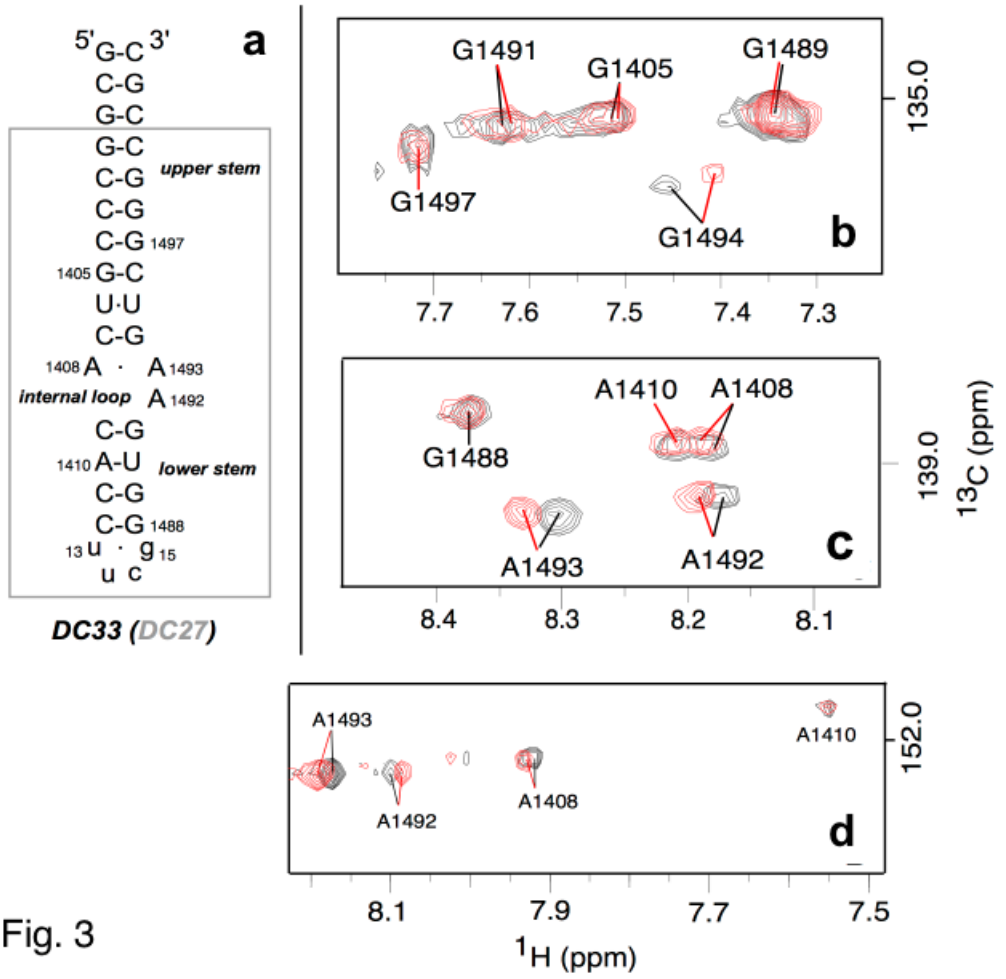
5'G-C 3'
a
C-G
G-C
G-C
C-G
upper stem
C-G
C-G
C-G 1497
1405 G-C
U·U
C-G
1408 A · A 1493
internal loop A 1492
C-G
1410 A-U
lower stem
C-G
C-G 1488
13 u · g 15
u c
DC33 (DC27)
G1491
G1405
G1489
G1497
G1494
b
135.0
7.7
7.6
7.5
7.4
7.3
A1410
A1408
G1488
A1493
A1492
c
139.0
13C (ppm)
8.4
8.3
8.2
8.1
A1493
A1410
A1492
A1408
d
152.0
8.1
7.9
7.7
7.5
1H (ppm)

Fig. 3

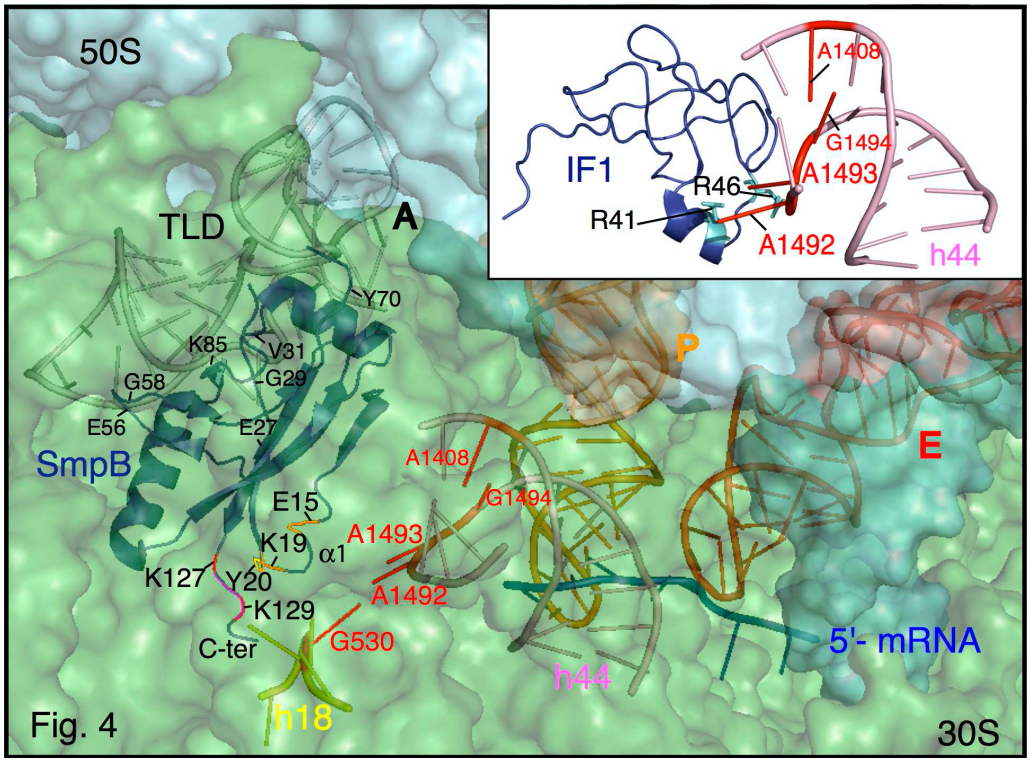
50S
TLD
A
Y70
K85
V31
G58
G29
E56
E27
SmpB
E15
K19
α1
K127
Y20
K129
C-ter
h18
A1408
G1494
A1493
A1492
G530
h44
P
E
5'- mRNA
30S
IF1
R46
R41
A1408
G1494
A1493
A1492
h44

Fig. 4